

Article

Optimization of Sustainable Production Processes in C45 Steel Machining Using a Confocal Chromatic Sensor

Jozef Jurko ¹, Katarína Paľová ², Peter Michalík ³ and Martin Kondrát ^{1,*}

¹ Department of Industrial Engineering and Informatics, Faculty of Manufacturing Technologies, Technical University of Košice, Bayerova 1, 08001 Prešov, Slovakia; jozef.jurko@tuke.sk

² Department of Biomedical Engineering and Measurement, Faculty of Mechanical Engineering Technical University of Košice, Letná 9, 04200 Košice, Slovakia; katarina.palova@student.tuke.sk

³ Department of Automotive and Manufacturing Technologies, Faculty of Manufacturing Technologies, Technical University of Košice, Štúrova 31, 08001 Prešov, Slovakia; peter.michalik@tuke.sk

* Correspondence: martin.kondrat@tuke.sk; Tel.: +421-55-602-6420

Abstract: Metal machining production faces a myriad of demands encompassing ecology, automation, product control, and cost reduction. Within this framework, an exploration into employing a direct inspection of the machined area within the work zone of a given machine through a confocal chromatic sensor was undertaken. In the turning process, parameters including cutting speed (A), feed (B), depth of cut (C), workpiece length from clamping (D), and cutting edge radius (E) were designated as input variables. Roundness deviation (Rd) and tool face wear (KM) parameters were identified as output factors for assessing process performance. The experimental phase adhered to the Taguchi Orthogonal Array L27. Confirmatory tests revealed that optimizing process parameters according to the Taguchi method could enhance the turning performance of C45 steel. ANOVA results underscored the significant impact of cutting speed (A), feed (B), depth of cut (C), and workpiece length from clamping (D) on turning performance concerning Rd and KM . Furthermore, initial regression models were formulated to forecast roundness variation and tool face wear. The proposed parameters were found to not only influence the machined surface but also affect confocal sensor measurements. Consequently, we advocate for the adoption of these optimal cutting conditions in product production to bolster turning performance when machining C45 steel.



Citation: Jurko, J.; Paľová, K.; Michalík, P.; Kondrát, M.

Optimization of Sustainable Production Processes in C45 Steel Machining Using a Confocal Chromatic Sensor. *Lubricants* **2024**, *12*, 99. <https://doi.org/10.3390/lubricants12030099>

Received: 13 January 2024

Revised: 5 March 2024

Accepted: 14 March 2024

Published: 16 March 2024



Copyright: © 2024 by the authors. Licensee MDPI, Basel, Switzerland. This article is an open access article distributed under the terms and conditions of the Creative Commons Attribution (CC BY) license (<https://creativecommons.org/licenses/by/4.0/>).

Keywords: confocal chromatic sensor (CCHS); turning; steel C45; roundness deviation; tool face wear; machined surface; Taguchi method; ANOVA

1. Introduction

Laser scanning technology has been well established for several years, with its efficacy in product inspection demonstrated across various research endeavors. While the utilization of scanners in inspecting machined surfaces within the working zone of machines post process completion offers numerous benefits, it also presents limitations [1]. Sustainable and efficient manufacturing serves as the impetus behind the burgeoning Zero Defect Manufacturing (ZDM) trend. ZDM aims not only to detect defective products but also to predict and prevent defects [2]. As concluded by the authors of [3], dry machining proves optimal for clean manufacturing. Laser technology currently finds critical applications in the non-contact inspection of product parameters, with researchers exploring the integration of laser sensors in measuring parameters within the cutting zone during machining. According to [4], CCHS represents a high-precision measuring device, with data analysis stability outweighing mere accuracy. Reflectivity of the beam from the object to be measured and light source fluctuation pose challenges, as noted by [5]. Other researchers [6] delved into the utilization of CCHS in three-dimensional product surface measurement. Meanwhile, in their exploration of product measurement, Ref. [7] employed a high-speed 3D camera system. The authors of [8] investigated the application of CCHS for assessing

the surface properties of product layers in [9]. However, the machining process itself can be significantly influenced by factors such as surface topography and microhardness [10–12], surface roughness [10,11,13], residual stress [14–16], and microstructure [17]. In their analysis in [18], the authors provide insights and solutions for machining hardened steels with regard to surface integrity. Specifically, they explore the impact of hardening on surface roughness, cylindricity, and roundness after turning C45 steel. Research findings [19] indicate a detrimental effect of hardening on surface quality. Furthermore, surface treatment via machining methods can alter parameters associated with surface integrity [20]. The investigation and analysis of the surface quality parameters of milled surfaces were conducted using a confocal laser scanning microscope by the authors of [21]. Mechanical hardening is described in detail in studies by the authors of [22,23]. Additionally, other researchers have endeavored to identify the influence of material properties on the surface hardening of materials such as Al 6061-T6 [24] and Hadfield steels [25–31]. The issue of surface hardening in AISI 304 steel is addressed in [32]. The authors of [33] examine samples of surface roughness after turning. The influence of surface texture on surface roughness is investigated in [34], while Ref. [35] analyzes the impact of the tip radius of measuring contacts on surface roughness parameters. Additionally, Ref. [36] asserts results that surface roughness significantly affects machined product performance. Investigations into factors affecting the machined surface of metallic materials are carried out by the authors of [37,38]. The authors of [39] observe the deterioration of machined surfaces in Ti6Al4V alloys due to thermal softening using the HSM method. Similarly, results from [40] indicate a trade-off relationship between significant process factors' influence on material removal rate and surface roughness. Regarding EDM technology, Ref. [41] investigates the performance of machined stainless steel. Changes in machined surfaces affect quality parameter attainment in milling due to thermal deformation [42], in turning due to stress and strain prediction [43], in turning due to cutting tool modification [44] and cutting tool damage [45], and in milling Ti alloys due to elastic deformation [46]. The investigation of the effect of tool wear on surface roughness increase is addressed by [47], while [48] demonstrates through research that low-temperature cooling can enhance machined surface quality while minimizing tool wear. The determination of tool wear in the machining of duplex stainless steel is presented in papers [49,50], with the issue of tool wear and surface topography also discussed in [51–55]. Additional researchers [56] conduct experimental investigations into factors affecting stainless steel turning and assess wear parameters on the cutting tool's face and back surface. Additionally, surface integrity evaluation parameters encompass shape and position deviations. In this regard, the application of CCHS proves highly beneficial, particularly considering its comprehensive data and swift data acquisition. Nonetheless, the challenge remains in efficiently processing acquired data and accurately interpreting them for theoretical and practical needs, as per the research results in [1]. The authors of [57] utilize CCHS to measure roundness deviation and demonstrate, through experimental results, the method's steady and reliable evaluation of roundness deviations. Several authors have explored different machinability characteristics of C45 steel through varying heat treatment methods [58], employing coated tools in milling [59], utilizing process media [60], implementing ultrasonics in turning [61], and modifying cutting inserts [62]. Furthermore, the authors of [63–65] investigate various parameters of machined surfaces using non-contact methods.

Our primary research focus revolves around controlling factors affecting machined surfaces through non-contact methods, utilizing laser sensors directly within a machine's working zone. We aim to optimize input parameters and analyze adverse phenomena on machined surfaces.

In this investigation, we explored the feasibility of directly measuring roundness deviation within a machine's working zone using a confocal chromatic sensor during the turning of C45 steel. In the turning process, parameters such as cutting speed (A), feed (B), depth of cut (C), workpiece length from clamping (D), and cutting edge radius (E) were chosen as input parameters. Roundness deviation and tool face wear (KM) parameters,

following ISO 3685 standards, were proposed as output factors for evaluating process performance, measured using a microscope. To measure roundness deviation, we developed new-generation CCHS sensors (CL P070 from Keyence—Mechelen, Belgium). To analyze the effect of cutting insert face wear on roundness deviation under defined cutting conditions using Taguchi Design in Minitab 21.4.2 software, we designed the Orthogonal Array L27 experiment matrix. All research tests were conducted under dry turning conditions, with a key assumption being that machine tool vibrations align with prescribed values certified for specific machine tools (as outlined in Table 1). Currently, several companies in our region manufacture various C45 steel products for the engineering industry.

Table 1. Experimental data.

M—Machine	Leadwell T5 CNC machine tool equipped with a FANUC Oi-MATE-TC control system. Maximum radial sweep certified by the manufacturer is 0.030 mm, and maximum axial sweep is 0.020 mm.
T—Cutting insert Tool holder Working insert tool geometry	Cutting tool clamped with a tool holder marked SSDCN1212 F09 from Dormer Pramet Ltd., Šumperk, Czech Republic. Cutting insert SCMT 09T308E-FM, T9325 made of sintered carbide, with specific geometry parameters (nose angle $\epsilon_r = 90^\circ$, main cutting edge setting angle $\kappa_r = 45^\circ$, clearance angle major $\alpha = 7^\circ$, and nose radius $r_\epsilon = 0.8$ mm).
W—Workpiece material and dimensions	Workpiece material C45 steel (1.0503). Test specimen dimensions: diameter (d) = 40 mm, length (L) = 150 mm. The chemical composition of the steel is given in Table 2 and was verified prior to the start of the research. Table 3 shows the main properties of the tested steel.
F—Fixture for tool and object	Specimen: A round bar clamped in a chuck. Tool: Clamped in the cutter head.
Machining conditions	Dry machining. Machining method—turning.
Mobile Measuring System (MMS) is composed of CCHS sensor	PLC Siemens-1511C, Communication module KEYENCE-CL3000, Amplifier KEYENCE-CLP070N, Communication module KEYENCE-DL-PN1 and sensor CL P070 by Keyence. Measurement range: 75 mm to 130 mm. Reference distance: 100 mm. Resolutions: ± 1 mm. Spot diameter: 600 mm. Linearity: $\pm 0.15\%$ of F.S. (IL-100: ± 20 mm). Repeatability: 4 mm. For the research purposes, a bespoke holder tailored for the CCHS sensor was meticulously designed and subsequently fabricated utilizing advanced 3D printing technology.

Table 2. Chemical composition of C45 steel (EN 10083-2-91) *.

Steel C45	(%)
C	0.50
Mn	0.80
Si	0.37
Cr	0.22
Ni	0.28
Cu	0.18
P	0.035
S	0.032

* Chemical composition verified through analysis of the sample.

Table 3. Verified properties of C45 steel products.

Steel C45	Values
Yield stress Re (MPa)	202
Tensile strength Rm (MPa)	650
Density (g/cm ³)	7.85
Hardness HB	max. 220
Elastic modulus (GPa)	81
Flexural strength (MPa)	606
Thermal conductivity (W/mK)	50

2. Description, Implementation, and Experimental Results

2.1. Experimental Design

In this section, we outline the experimental setup and methodology employed in our study. We proposed to utilize the experimental data within the framework of the technology system (TS) depicted in Figure 1, along with the mobile measurement system (MMS) previously introduced by the authors [1], illustrated in Figure 2 and described in detail in Table 1. The experimental parameters considered in this study are enumerated in Table 1. The range for each controlled parameter was determined based on prior experiments and information obtained from manufacturers of C45 steel products, as summarized in Table 2. Additionally, adhering to recommendations from the tool manufacturer, a specific cutting insert was selected for machining C45 steel, as detailed in Table 1.



Figure 1. Technological System (TS). The TS comprises the machine (M), tool (T), workpiece (W), and fixture (F).



Figure 2. Mobile Measuring System (MMS).

The cutting process conditions are outlined in Table 4, with cutting speed designated as parameter A, feed as parameter B, depth of cut as parameter C, workpiece length from clamping as parameter D, and cutting edge radius as parameter E. The assessment of the output factor, specifically the roundness deviation of the circular bar, was conducted using CCHS. The experimental matrix and resultant output factors, represented as average values from the measurements, are detailed in Tables 5 and 6. Roundness deviation of

the machined surface was directly measured and analyzed within the working zone of the machine tool utilizing CCHS. This measurement was performed post-machining on a 240 mm length workpiece without unclamping, employing MMS (mobile measurement system) for CCHS. *Rd* was assessed at three points along the machined length (60 mm) of the circular bar, specifically at distances of 5.0 mm, 30.0 mm, and 55.0 mm from the clamping point (refer to Figure 3). *KM* face wear was gauged following a 240 mm traversal, adhering to ISO 3685 [66] standards, as illustrated in Figure 4. *Rd* values for specific local locations were determined as averages. Resultant average values of *Rd* and cutting insert face wear were derived from 12 replicate measurements, with the exclusion of minimum and maximum outliers. Each experiment employed a cutting insert with a new cutting edge. Literature reviews [55,56] highlight the importance of surface integrity research incorporating new technologies, necessitating further investigation. The exploration of roundness deviation control using CCHS on a reference specimen of C45 steel serves as a foundation for other materials. A systematic examination of process parameter effects on the machined surface underscores the potential to influence output factors towards desired values by parameter adjustments. Enhanced machined surface integrity is achievable through the optimization of input parameters such as cutting speed, feed, depth of cut, workpiece clamping length, and cutting edge radius. The alignment of cutting conditions with CCHS requirements is imperative. These adjustable input parameters during turning render them conducive to automation and intelligent processing.

Table 4. The primary machining conditions.

Symbol	Process Parameters Units	Levels		
		1	2	3
A	Cutting speed (m/min)	90	180	270
B	Feed (mm/rev.)	0.1	0.2	0.3
C	Depth of cut (mm)	0.1	0.4	0.8
D	Workpiece length from clamping (mm)	5.0	30.0	55.0
E	Cutting edge radius (mm)	0.003 + 0.0005	0.005 + 0.0005	0.008 + 0.0005

Table 5. Experimental matrix, design, and experimental results.

Number of Exp.-RUN	Controllable Process Parameter					Experimental Results			
	A	B	C	D	E	<i>Rd</i> (mm)			<i>KM</i> (mm)
						Average <i>Rd</i>	STDVP	STDV ERROR SE (AVERAGE)	
1	1	1	1	1	1	0.0260	0.001	0.0003	0.1420
2	1	1	1	1	2	0.0184	0.001	0.0005	0.1120
3	1	1	1	1	3	0.0220	0.001	0.0006	0.1180
4	1	2	2	2	1	0.0440	0.001	0.0006	0.1850
5	1	2	2	2	2	0.0440	0.002	0.0009	0.1740
6	1	2	2	2	3	0.0410	0.001	0.0006	0.1670
7	1	3	3	3	1	0.0860	0.005	0.0024	0.1820
8	1	3	3	3	2	0.0720	0.003	0.0015	0.1810
9	1	3	3	3	3	0.0640	0.003	0.0012	0.1960
10	2	1	2	3	1	0.0520	0.003	0.0012	0.1730
11	2	1	2	3	2	0.0450	0.002	0.0010	0.1710
12	2	1	2	3	3	0.0460	0.013	0.0059	0.1690
13	2	2	3	1	1	0.0640	0.008	0.0035	0.1860
14	2	2	3	1	2	0.0420	0.012	0.0054	0.1820
15	2	2	3	1	3	0.0390	0.011	0.0051	0.1670
16	2	3	1	2	1	0.0340	0.005	0.0025	0.1750
17	2	3	1	2	2	0.0360	0.007	0.0030	0.1700
18	2	3	1	2	3	0.0320	0.003	0.0012	0.1710
19	3	1	3	2	1	0.0370	0.010	0.0043	0.1880
20	3	1	3	2	2	0.0410	0.001	0.0006	0.1770
21	3	1	3	2	3	0.0390	0.003	0.0013	0.1860
22	3	2	1	3	1	0.0300	0.007	0.0031	0.1970
23	3	2	1	3	2	0.0370	0.008	0.0034	0.1820
24	3	2	1	3	3	0.0440	0.010	0.0045	0.1820
25	3	3	2	1	1	0.0290	0.001	0.0004	0.1820
26	3	3	2	1	2	0.0370	0.002	0.0007	0.1920
27	3	3	2	1	3	0.0180	0.002	0.0009	0.1810

Table 6. Calculated *S/N* ratios.

Number of Exp.-RUN	<i>S/N</i> Ratios of Results	
	<i>Rd</i> (dB)	<i>KM</i> (dB)
1	31.7005	16.9542
2	34.7036	19.0156
3	33.1515	18.5624
4	27.1309	14.6566
5	27.1309	15.1890
6	27.7443	15.5457
7	21.3100	14.7986
8	22.8534	14.8464
9	23.8764	14.1549
10	25.6799	15.2391
11	26.9357	15.3401
12	26.7448	15.4423
13	23.8764	14.6097
14	27.5350	14.7986
15	28.1787	15.5457
16	29.3704	15.1392
17	28.8739	15.3910
18	29.8970	15.3401
19	28.6360	14.5168
20	27.7443	15.0405
21	28.1787	14.6097
22	30.4576	14.1107
23	28.6360	14.7986
24	27.1309	14.7986
25	30.7520	14.7986
26	28.6360	14.3340
27	34.8945	14.8464

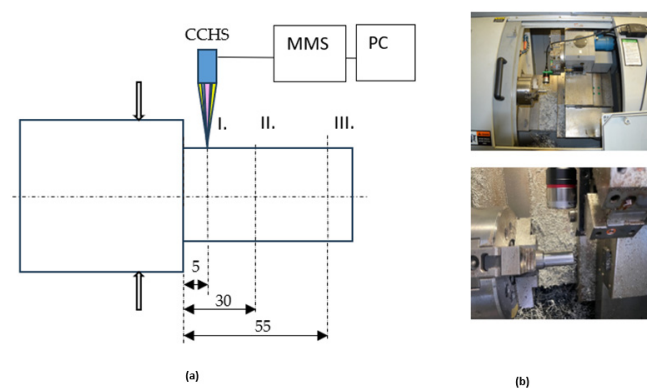


Figure 3. The measurement layout within the Leadwell T5 CNC machine zone. (a) Measurement scheme utilizing CCHS (confocal chromatic sensor), MMS (Mobile Measuring System), and PC (Personal Computer). (b) Visualization of the working area of the CNC machine.

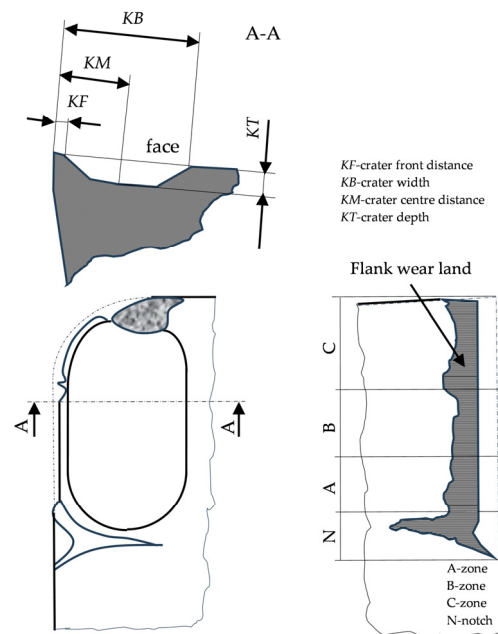


Figure 4. The cutting tool wear parameters as per ISO 3685 [66].

The face wear on the cutting insert was assessed in accordance with ISO standard 3685, as depicted in Figure 4, and analyzed by using a Carl Zeiss Primotech D/A ESD microscope – Carl Zeiss Jena GmbH, Jenna, Germany as shown in Figure 5.

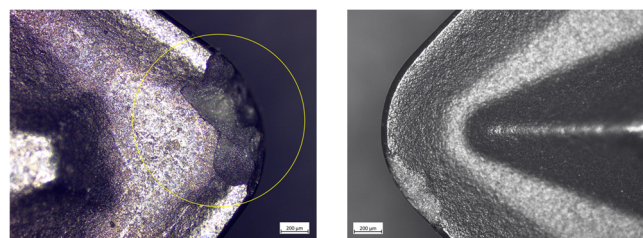


Figure 5. The measurement of wear on the cutting insert face employing a Carl Zeiss Primotech D/A ESD microscope. Magnification $5\times$ The yellow circle characterizes the face wear of tool.

2.2. Optimization of Turning Input Parameters Using Taguchi Method with S/N Ratio Analysis

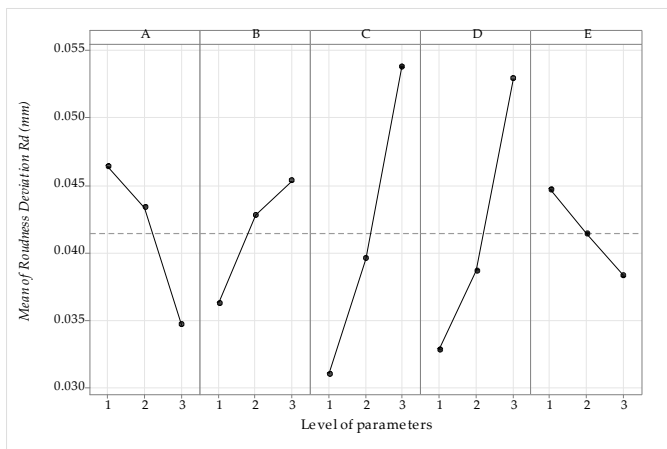
An experiment matrix employing Orthogonal Array L27 was designed following Taguchi principles using Minitab 21.4.2 software—Coventry, United Kingdom. Five parameters were set at three levels each, resulting in a total of 27 runs.

Researchers [67,68] have noted that Taguchi's methodology [69] considers factors such as resource wastage, warranty costs, customer complaints, and repair expenses, all of which influence product quality. Taguchi's approach is particularly beneficial for optimizing products or processes while simultaneously reducing experimentation time and research costs. Orthogonal arrays, coupled with signal-to-noise ratio analysis, are employed to gauge output parameter quality. Various models incorporating Taguchi methods have been applied in research, with parameters' significance determined through ANOVA. These models include L8OA [70–72], L18OA [73], L27OA [74,75], L27OA with ANOVA [58,76,77], L18OA with ANOVA [78], L9OA with ANOVA [37,60,72], and the L8OA model combined with Response Surface Methodology (RSM) and ANOVA [38,79,80]. Additionally, the GRA (Grey Relation Analysis) method with ANOVA has been proposed [74,81–84], along with other variations by different researchers [85].

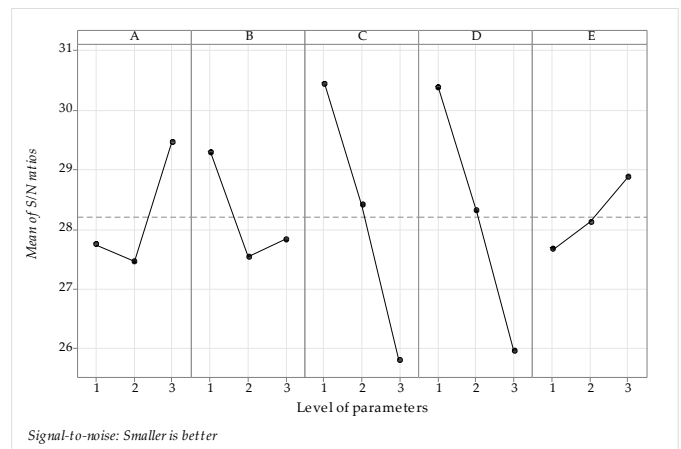
Genichi Taguchi [69] introduced a loss function in data processing to represent the disparity between experimental and target values, subsequently converted into signal-to-noise (S/N) ratios. The S/N ratio, defined as the ratio of mean value to standard deviation,

categorizes into “Larger is Better,” “Medium is Better,” and “Smaller is Better,” based on response requirements. This study focuses on the output factors of roundness deviation and wear on the cutting insert’s face surface, both adopting the “Smaller is Better” methodology, aligned with practical and C45 steel machinability requirements. Equation (1) was utilized for S/N ratio calculation, with the results tabulated in Table 6. Taguchi analysis, mean S/N ratio graphs, and ANOVA were conducted using Minitab 21.4.2 software.

The impact severity of each input parameter on output factors is depicted in Figures 6 and 7. Cutting conditions and cutting insert geometry influence chip evacuation from the cutting zone [37,43,44,78]. Continuous cutting processes yield regular machined surfaces devoid of Plastically Deformed Material (PDM) elements. Conversely, discontinuous cutting may produce irregular chips with PDM, adversely affecting surface quality and increasing roundness deviation (see Figure 6). Increasing Rd may signify elevated cutting insert wear, notably on the KM face, further exacerbating surface quality due to augmented PDM elements.

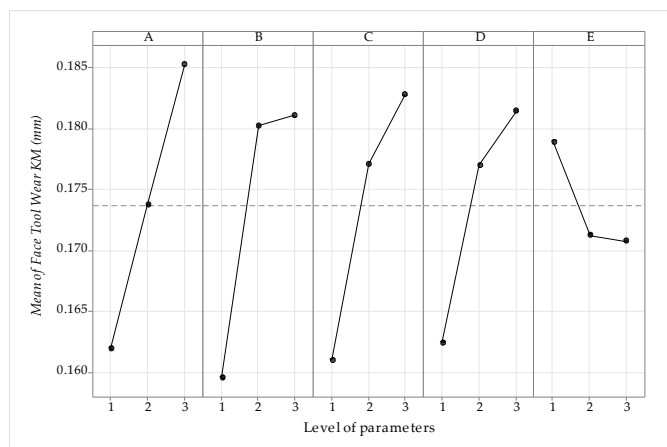


(a)

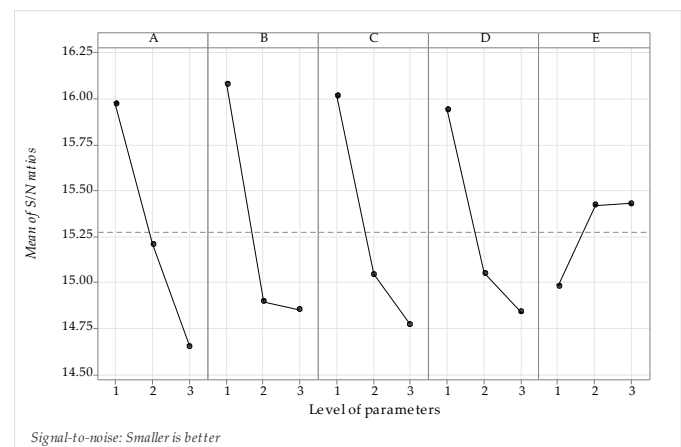


(b)

Figure 6. Main effects plots: (a) illustrates the effects of input factors on roundness deviation, while (b) displays the mean S/N ratios corresponding to roundness deviation.



(a)



(b)

Figure 7. Main effects plots: (a) the effects of input factors on the tool wear of the face, and (b) the mean S/N ratios corresponding to the tool wear of the face.

The S/N ratio (Equation (1)) serves as a quantitative tool, with Rd proposed as a qualitative machined surface factor, ideally minimized. The S/N ratio is as follows:

$$S/N = -10 \log \left[\frac{1}{n} (y_1^2 + y_2^2 + \dots + y_n^2) \right] \quad (1)$$

where

S/N represents parameter values (unit dB)

and

y_1, y_2, \dots, y_n are the observed output values for the test condition repeated n times.

Figures 6a and 7a depict the relationship between mean values of roundness deviation and the face wear of the cutting insert. Cutting speed emerges as the most influential parameter impacting roundness deviation (as evident in Figure 6a), similarly affecting tool wear at the cutting insert face (as observed in Figure 7a). Increased feed, depth of cut, and distance of the workpiece from the fixture also exert a negative effect on Rd . With rising roundness deviation, surface quality diminishes, accompanied by increased tool wear. Elevated cutting speed mitigates roundness deviation but heightens the risk of tool damage and wear. Optimal regions lie between cutting speed levels 1 and 2, as illustrated in Figures 6b and 7b. Figures 6a and 7a highlight the optimal levels of individual parameters to achieve the desired output factors in terms of roundness deviation (Rd) and the face wear of the cutting inserts, respectively. These optimal levels correspond to A3B1C1D1E3 for Rd and A1B1C1D1E3 for the face wear of the cutting inserts, as corroborated by the S/N ratio values in Figures 6b and 7b.

Lower roundness deviation (Rd) values can enhance the operational reliability of the studied functional surface of a product. This improvement stems from increased friction between the tool and workpiece, resulting in higher cutting temperatures with increasing cutting speed. Elevated temperatures in the machining zone cause thermal softening of the workpiece, reducing smeared materials on the machined surface and consequently minimizing roundness deviation [77,85,86]. As depicted in Figure 8, Rd values escalate with rising cutting speed due to heightened tool resistance against the workpiece, particularly as feed increases, leading to the formation of more built-up edges (BUE) on the tool face. This phenomenon induces surface deterioration and consequently elevates Rd values. Moreover, an increasing trend in Rd values accompanies higher depths of cut. These trends align with the existing literature findings on machining difficult-to-machine materials [87]. Precision in determining the local measurement spot on the specimen significantly influences Rd .

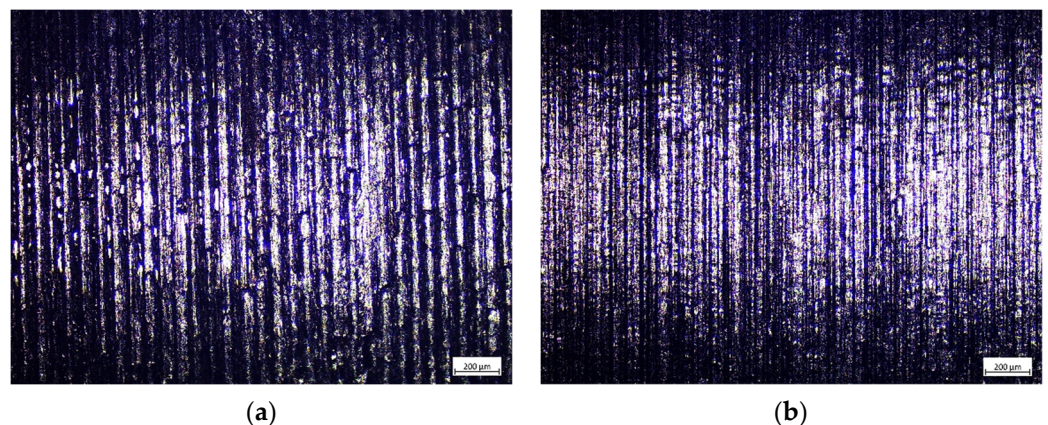


Figure 8. Visualization of machined surface. (a) Initial parameter settings at A = 180 m/min, B = 0.2 mm/rev., C = 0.4 mm, D = 30 mm, and E = 0.005 mm, (A2B2C2D2E2). Magnification 5×. (b) Taguchi optimum settings at A = 270 m/min, B = 0.1 mm/rev., C = 0.1 mm, D = 5.0 mm, and E = 0.008 mm, (A3B1C1D1E3). Magnification 5×.

Simultaneously, this measurement process provides insights into the cutting tool's compliance with the specified technical requirements of the product and identifies any undesirable wear. Variations in Rd magnitude may indicate changes in the cutting tool. Consequently, this measurement method facilitates the rapid and accurate identification of local spots on the functional surface and enables the monitoring of changes in cutting tool wear rate. However, the mean values of output factors are contingent on specific conditions, necessitating test repetition for other materials.

The S/N ratio response factor table for Rd is presented in Table 7. Figure 7b illustrates the S/N ratio chart generated using Minitab software. A higher S/N ratio indicates minimal deviation between the desired and measured outputs. As depicted in Figure 9b, the highest average S/N ratio values obtained for Rd are 270 m/min, 0.1 mm/rev., 0.1 mm, 5.0 mm, and 0.008 mm. Therefore, the assumed optimal process parameters for achieving low Rd using Taguchi's method are 270 m/min, 0.1 mm/rev., 0.1 mm, 5.0 mm, and 0.008 mm. These optimal combinations are highlighted in bold in Table 6 for clarity, with the corresponding levels identified. This predicted optimal combination is represented as A3B1C1D1E3 for roundness deviation.

Table 7. Mean S/N ratio response table for roundness deviation.

Symbol	Process Parameters and Units	Mean S/N Ratios				
		Level 1	Level 2	Level 3	Max–Min	Rank
A	Cutting speed (m/min)	27.73	27.45	29.45	2.00	3
B	Feed (mm/rev.)	29.28	27.54	27.83	1.74	4
C	Depth of cut (mm)	30.44	28.41	25.80	4.64	1
D	Workpiece length from clamping (mm)	30.38	28.30	25.96	4.42	2
E	Cutting edge radius (mm)	27.66	28.12	28.87	1.21	5

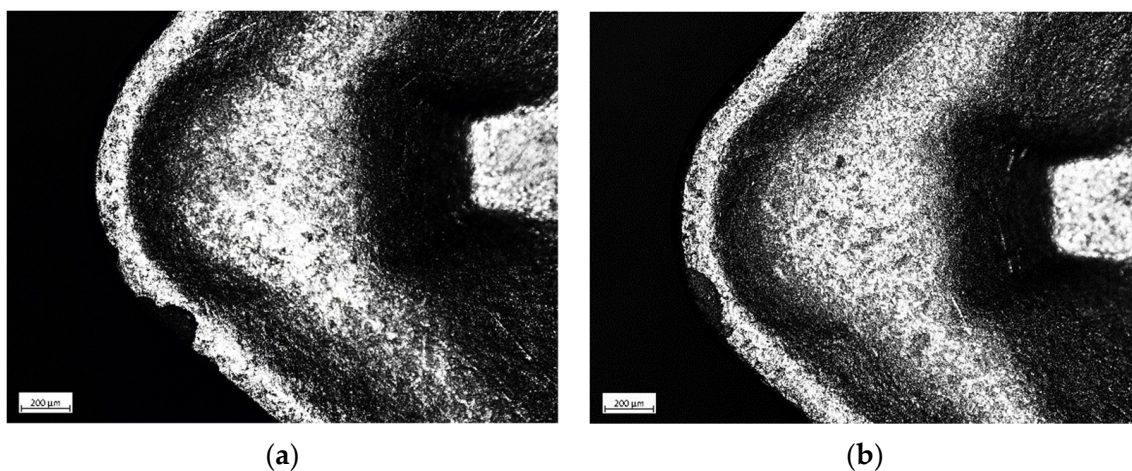


Figure 9. Wear display on cutting insert face. (a) Initial parameter settings at A = 180 m/min, B = 0.2 mm/rev., C = 0.4 mm, D = 30 mm, and E = 0.005 mm, (A2B2C2D2E2). Magnification 5 \times . (b) Taguchi optimum settings at A = 90 m/min, B = 0.1 mm/rev., C = 0.1 mm, D = 5.0 mm, and E = 0.008 mm, (A1B1C1D1E3). Magnification 5 \times .

Table 8 presents the generated S/N ratio factor table for face wear on the cutting insert. Mean values of the S/N ratio for face wear are depicted in Figure 7b. Based on the data from Figure 7b and Table 8, the estimated optimal process parameters for minimizing face wear are 90 m/min, 0.1 mm/rev., 0.1 mm, 5.0 mm, 0.008 mm. This predicted optimal combination is represented as A1B1C1D1E3 for face wear on the cutting insert.

Table 8. Mean S/N ratio response table for tool face wear.

Symbol	Process Parameters and Units	Mean S/N Ratio				
		Level 1	Level 2	Level 3	Max–Min	Rank
A	Cutting speed (m/min)	15.97	15.21	14.65	1.32	1
B	Feed (mm/rev.)	16.08	14.89	14.85	1.23	3
C	Depth of cut (mm)	16.01	15.04	14.77	1.24	2
D	Workpiece length from clamping (mm)	15.94	15.05	14.84	1.10	4
E	Cutting edge radius (mm)	14.98	15.42	15.43	0.45	5

The S/N ratio response table for Rd is also presented in Table 7, while Figure 6b illustrates the mean S/N ratio chart obtained through Minitab software—Coventry, United Kingdom. Again, a higher S/N ratio signifies minimal deviation between the desired and measured outputs. As indicated in Figure 6b, the highest average S/N ratio values obtained for Rd are $A3 = 270$ m/min, $B1 = 0.1$ mm/rev., $C1 = 0.1$ mm, $D1 = 5.0$ mm, and $E3 = 0.008$ mm. Thus, the assumed optimal process parameters for achieving low roundness deviation using Taguchi’s method are represented as $A3B1C1D1E3$, with the corresponding level values highlighted in bold in Table 7. Table 8 presents the obtained S/N ratio response table for face wear on the cutting insert. The average S/N ratio values for the face wear of the cutting insert are illustrated in Figure 7b. From Figure 7a, it can be observed that the estimated optimum process parameters for achieving low wear on the cutting insert face are $A1 = 90$ m/min, $B1 = 0.1$ mm/rev., $C1 = 0.1$ mm, $D1 = 5.0$ mm, and $E3 = 0.008$ mm.

Confirmation Test

To validate the optimality of the predicted optimal settings according to Taguchi, confirmatory tests must be conducted. The predicted signal-to-noise (S/N) ratio (ϵ) was utilized to estimate and verify the response under the predicted optimal cutting settings, calculated using Equation (2).

$$\epsilon_{predicted} = \epsilon_{tm} + \sum_{i=1}^p (\epsilon_o - \epsilon_{tm}) \quad (2)$$

where

ϵ_{tm} is the total mean S/N ratio;

ϵ_o is the mean S/N ratio at the optimal level;

p is the number of input process parameters.

Confirmatory tests are essential to validate the predicted optimal cutting settings.

After predicting the optimum cutting settings, confirmation experiments were conducted, and the results are presented in Tables 9 and 10 for Rd and KM , respectively. The predicted optimal cutting settings for both Rd and KM led to improved process performance outcomes. Tables 9 and 10 demonstrate that the S/N ratios under the predicted and optimal cutting settings closely align for both Rd and KM . The enhancement in the S/N ratio at the optimal cutting settings for Rd and KM amounted to 4.95 dB and 2.01 dB, respectively, compared to the original parameter settings shown in Tables 9 and 10. From the confirmation experiments, it was observed that the predicted optimal cutting settings by Taguchi yielded favorable results compared to the initial parameter settings, particularly with regard to the reduction in Rd and KM . Specifically, the reductions in Rd and KM compared to the initial parameter settings were found to be 15.29% and 12.5%, respectively. Hence, the predicted optimal cutting settings by Taguchi are deemed to be the optimum conditions for achieving low Rd and low KM in machining C45 steel under the given conditions. From Figures 8 and 9, it is evident that the optimal cutting settings as per Taguchi led to low Rd and KM values. Figure 10 demonstrates the reduced impact of removed material and fewer smeared particles on the machined surface under the optimum cutting conditions

according to Taguchi compared to the initial setup. Similarly, less face wear (smaller pitting) was observed at the optimal cutting setting by Taguchi compared to the initial setting.

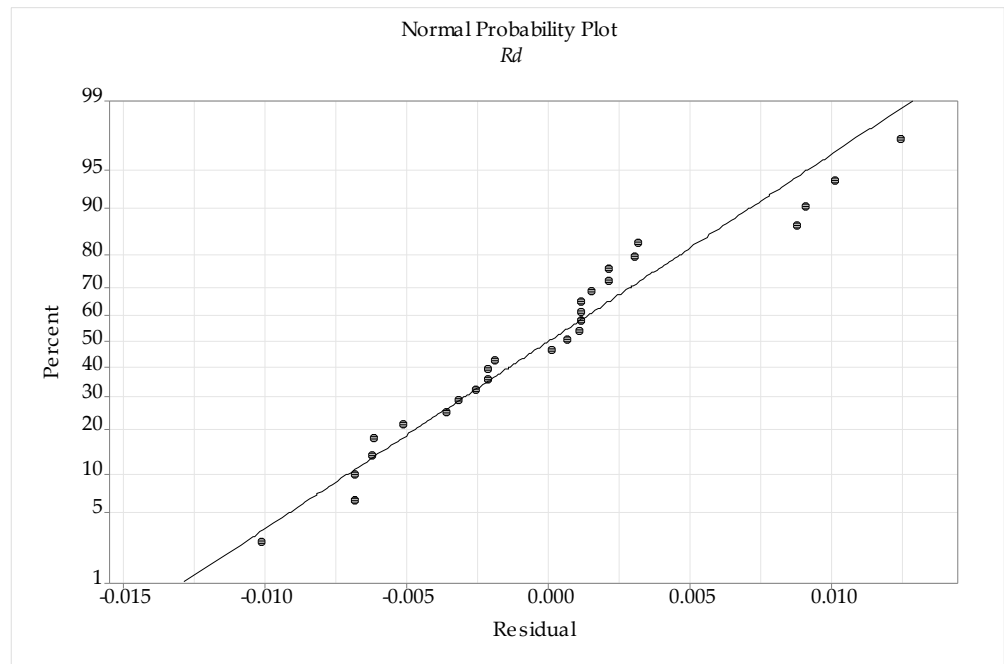


Figure 10. Normal probability plot of the residuals for roundness deviation.

Table 9. Confirmation test results for roundness deviation.

	Initial Process Parameter	Optimal Process Parameters	
		Prediction	Experiment
Level	A2B2C2D2E2	A3B1C1D1E3	A3B1C1D1E3
Roundness deviation (mm)	0.041		0.024
S/N ratio (dB)	27.44	35.56	32.39
Improvement in S/N ratio (dB)	4.95		
Percentage reduction in tool face wear	15.29%		

Table 10. Confirmation test results for tool face wear.

	Initial Process Parameter	Optimal Process Parameters	
		Prediction	Experiment
Level	A2B2C2D2E2	A1B1C1D1E3	A1B1C1D1E3
Tool face wear (mm)	0.198		0.157
S/N ratio (dB)	14.07	15.97	16.08
Improvement in S/N ratio (dB)	2.01		
Percentage reduction in tool face wear	12.5%		

3. Optimization of Input Parameters by ANOVA, Regression Analysis, and Modeling

ANOVA identifies the process parameters most influencing performance characteristics. Table 11 presents the analysis of variance for the output factor of roundness deviation (R_d). It indicates that cutting speed, feed, depth of cut, and workpiece length from clamping significantly affect roundness deviation (with p -values less than 0.05 at a 95% confidence interval). However, the significance of the cutting edge radius of the curvature parameter regarding roundness deviation was not demonstrated. R_d is notably influenced by depth of cut (37.51%), workpiece length from clamping (30.29%), cutting speed (10.50%), and feed

(6.21%), while cutting edge radius exhibits the least significance (2.85%). Table 12 presents the analysis of variance for the output factor of cutting insert face wear. It indicates that cutting speed, feed, depth of cut, and length of workpiece from clamping significantly affect *KM* cutting insert face wear (with *p*-values less than 0.05 at a 95% confidence level). However, the significance of the cutting edge radius parameter for *KM* was not demonstrated. *KM* is significantly influenced by feed (25.43%), cutting speed (23.27%), depth of cut (21.83%), and workpiece length from clamping (16.89%), with cutting edge radius exhibiting the least effect (3.56%).

Table 11. Analysis of variance for roundness deviation.

Source	DF	Adj SS	Adj MS	F-Value	<i>p</i> -Value	Contribution	Remarks
A	2	0.000665	0.000332	6.65	0.008	10.50%	Significant
B	2	0.000393	0.000197	3.94	0.041	6.21%	Significant
C	2	0.002375	0.001187	23.76	0.000	37.51%	Significant
D	2	0.001917	0.000959	19.18	0.000	30.29%	Significant
E	2	0.000181	0.000090	1.81	0.196	2.85%	Insignificant
Error	16	0.000800	0.000050			12.63%	
Total	26	0.006330				100.00%	

Table 12. Analysis of variance for face wear.

Source	DF	Adj SS	Adj MS	F-Value	<i>p</i> -Value	Contribution	Remarks
A	2	0.002450	0.001225	20.63	0.003	23.27%	Significant
B	2	0.002678	0.001339	22.54	0.001	25.43%	Significant
C	2	0.002298	0.001149	19.34	0.005	21.83%	Significant
D	2	0.001778	0.000889	14.97	0.008	16.89%	Significant
E	2	0.000374	0.000187	3.15	0.070	3.56%	Insignificant
Error	16	0.000950	0.000059			9.03%	
Total	26	0.010528				100.00%	

In this study, Minitab 21.4.2 software was utilized to develop predictive mathematical models for the dependent variable of roundness deviation, considering cutting speed (A), feed (B), depth of cut (C), workpiece length from clamping (D), and cutting edge radius (E), through linear regression analysis. No transformation was applied to each response. The prediction equation obtained from the regression analysis for *Rd* (3) and *KM* (4) is provided below.

Regression analysis model for roundness deviation versus A, B, C, D, and E with regression Equation (3):

$$Rd = 0.00764 - 0.00586 A + 0.00453 B + 0.01137 C + 0.01003 D - 0.00317 E, \quad (3)$$

For *Rd*, an R^2 value of 83.81% was calculated.

Regression analysis model for face wear versus A, B, C, D, and E with regression Equation (4):

$$KM = 0.0961 + 0.01167 A + 0.01078 B + 0.01089 C + 0.00850 D - 0.00406 E, \quad (4)$$

For *KM*, an R^2 value of 81.64% was calculated.

The fitness of the developed models was validated using the coefficient of determination R^2 [88,89]. The coefficient of determination ranges from zero to one, where a value closer to one indicates a strong agreement between the dependent and independent variables. For instance, an R^2 value of 95% signifies that 95% of the variability in new observations has been estimated. In this study, the regression models for *Rd* and *KM* achieved high R^2 values, namely 83.81% and 81.64%, respectively.

A graph of the residuals was employed to assess the significance of coefficients in the predicted model. The linearity of the residual graph indicates that the residual errors in the model are normally distributed, and the coefficients are significant. Figure 10 displays the residuals for roundness deviation. It illustrates that the residuals closely align with a straight line, indicating the significance of the coefficients in the developed model. Similarly, Figure 11 depicts the residuals for tool face wear. The residuals also fall near a straight line, suggesting the significance of the coefficients in the developed model for *KM*. To validate the developed models, confirmatory tests were conducted, and the results are presented in Table 11. The test results, taken randomly from the orthogonal array L27, demonstrate good agreement between the predicted and experimental results across a range of parameters. The response was found to be favorable for machining different difficult-to-cut materials [74,75,81].

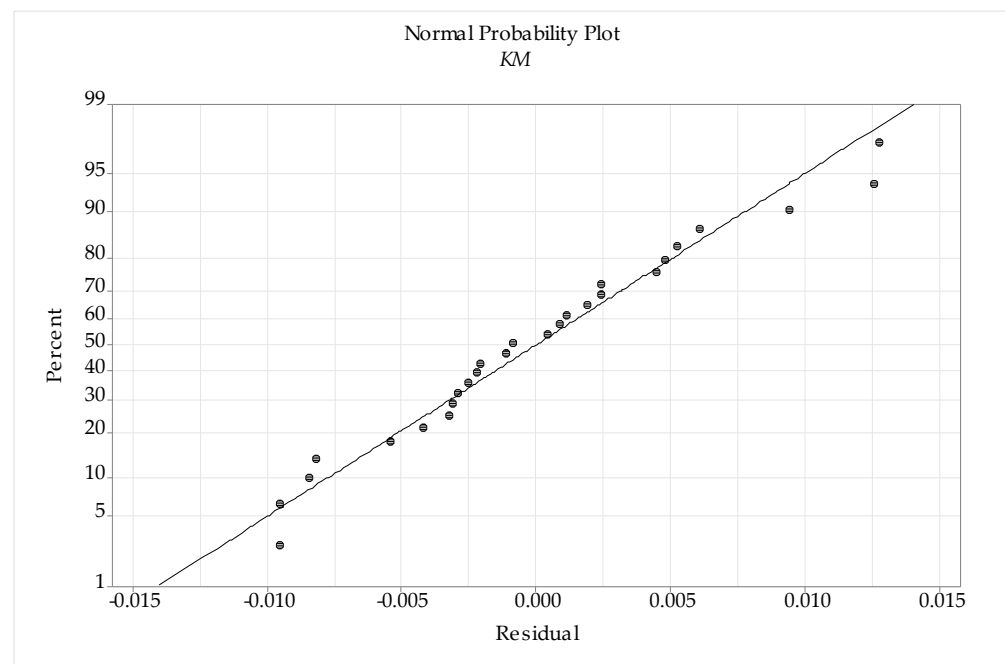


Figure 11. Normal probability plot of the residuals for tool face wear.

Confirmation Test

Confirmation tests of the control factors were conducted following the Taguchi method and regression equations for both the optimum level and randomly selected levels. Table 13 provides a comparison between the test results and the predicted values obtained using the Taguchi method and regression equations (Equations (3) and (4)). The proximity of the predicted values to the experimental values indicates a high level of agreement between them. To ensure reliable statistics in the analyses, the error values must be kept below 20% [88]. An examination of the results in terms of percentages reveals that the errors for the output factors of *Rd* and *KM* did not exceed the 20% threshold. Consequently, the results of the confirmatory test demonstrate a successful optimization process. According to the authors of [89,90], similar results were obtained during material machining processes, affirming the effectiveness of the Taguchi optimization method in enhancing the machining performance of C45 steel under the specified process parameters.

This validation process was conducted under both practical conditions, addressing the need for controlling the factors of machined surfaces, and under laboratory conditions, ensuring the reliability and robustness of the optimization procedure.

Table 13. Confirmation results for the developed models.

Run	Experimental		Predicted		Residuals		Error	
	<i>Rd</i> (mm)	<i>KM</i> (mm)	<i>Rd</i> (mm)	<i>KM</i> (mm)	<i>Rd</i> (mm)	<i>KM</i> (mm)	<i>Rd</i> (%)	<i>KM</i> (%)
1	0.026	0.112	0.025	0.122	0.001	−0.01	3.846	8.929
6	0.041	0.167	0.040	0.172	0.001	−0.005	2.439	2.994
10	0.052	0.173	0.051	0.176	0.001	−0.003	1.923	1.734
11	0.045	0.169	0.048	0.168	−0.003	0.001	6.667	0.592
16	0.034	0.167	0.037	0.175	−0.003	−0.008	8.824	4.79
19	0.037	0.188	0.042	0.189	−0.005	−0.001	13.513	0.532
23	0.037	0.182	0.036	0.184	0.001	−0.002	2.703	1.099
25	0.029	0.182	0.031	0.191	−0.002	−0.009	6.896	4.945

4. Conclusions

The discrepancies between the theoretical and actual values of the machined surface factors stem from the deformation process occurring ahead of the cutting edge of the tool. This process is primarily influenced by the properties of the material being machined and the prevailing working conditions [91–93]. The authors of [1,94] presented both positive and negative experiences regarding the use of CCHS in measuring roundness deviation on machined surfaces after turning C45 steel. Furthermore, this research uncovered several concomitant phenomena, including the following:

- Plastic deformation occurred at localized sites on the machined surface, as illustrated in Figure 12. These observations were captured using scanning electron microscopy with a JEOL JSM 7000F autoemission nozzle—JEOL Ltd., Hertfordshire, England, United Kingdom. The results of this analysis warrant further investigation.

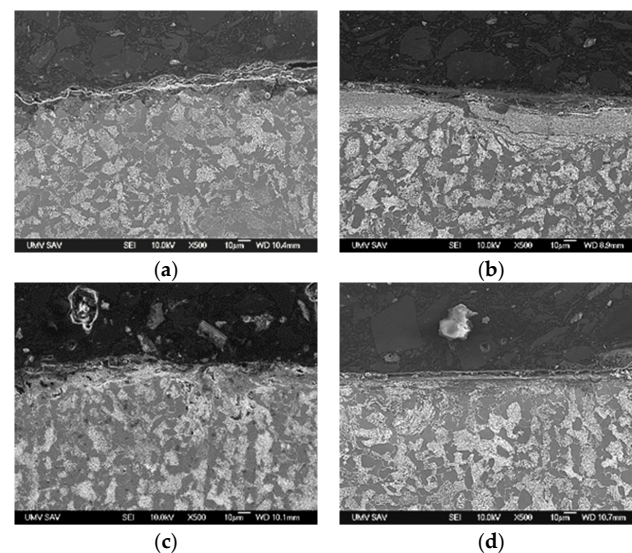


Figure 12. Examples of machined surfaces after turning C45 steel. (a) Deformation of the machined surface not measurable. Perlite and ferrite. Nital. Magnification 500 \times , A = 180 m/min, B = 0.2 mm/rev, C = 0.4 mm, D = 30 mm, E = 0.005 mm. (b) Local plastic deformation of machined surface \sim 34 μ m. Perlite and ferrite. Nital. Magnification 500 \times , A = 270 m/min, B = 0.1 mm/rev, C = 0.1 mm, D = 5.0 mm, E = 0.008 mm. (c) Local plastic deformation of machined surface. Traces of volume extraction of the machined surface. Perlite and ferrite. Nital. Magnification 500 \times , A = 180 m/min, B = 0.2 mm/rev, C = 0.4 mm, D = 30 mm, E = 0.005 mm. (d) Local plastic deformation of machined surface \sim 12 μ m. Perlite and ferrite. Nital. Magnification 500 \times , A = 90 m/min, B = 0.1 mm/rev, C = 0.1 mm, D = 5.0 mm, E = 0.008 mm.

The research presented in this paper offers several key conclusions based on the analysis conducted. The confocal chromatic sensor (CCHS) proved to be suitable for measuring the roundness deviation of machined surfaces, particularly on C45 steel. The data collected using CCHS can serve as a reference for further research, potentially extending to the comparison of other types of steels. Roundness deviation values were effectively measured and evaluated within the range of 0.002 to 0.08 mm using CCHS, aligning with the specified limit of 0.1 mm. The observed wear value on the cutting insert face reached up to 0.3 mm under the research conditions.

Key research findings include the following:

- The Taguchi method identified an optimal combination of cutting conditions ($A = 270$ m/min, $B = 0.1$ mm/rev., $C = 0.1$ mm, $D = 5.0$ mm, and $E = 0.008$ mm) resulting in a 53% reduction in roundness deviation.
- Similarly, Taguchi's method determined optimal cutting conditions ($A = 90$ m/min, $B = 0.1$ mm/rev., $C = 0.1$ mm, $D = 5.0$ mm, and $E = 0.008$ mm), leading to a 31% reduction in the face wear of the cutting insert.
- ANOVA analysis revealed that depth of cut had the most significant influence on roundness deviation (37.51%), followed by workpiece distance from clamping, cutting speed, and feed. Feed was found to be the most significant factor influencing tool cutting insert wear, with a percentage influence of 25.43%.

These results underscore the effectiveness of the determined optimal cutting settings in reducing roundness deviation and cutting insert face wear during the machining of C45 steel. The findings also highlight the potential of these optimal settings to positively impact roundness deviation.

Practical implications relevant for customers include the following:

- Fine-tuning conditions and controlling factors for laser sensor use on machined surfaces of C45 steel.
- The identification of negative phenomena on machined surfaces after turning C45 steel.
- The consideration of non-contact laser sensor methods for measuring the roundness deviation of machined surfaces in order to implement optimal cutting settings and enhance the quality of turning C45 steel within the specified range.

Author Contributions: Conceptualization, J.J., K.P., and P.M.; methodology, J.J. and P.M.; calculation, J.J.; validation, J.J. and K.P.; formal analysis, M.K.; investigation, J.J.; resources, P.M.; data curation, M.K.; writing—original draft preparation, J.J.; writing—review and editing, M.K.; visualization, M.K.; supervision, P.M. and J.J.; project administration, M.K.; funding acquisition, J.J. All authors have read and agreed to the published version of the manuscript.

Funding: This work was supported by the project AMTRteam (Advanced Manufacturing Technology Research Team), awarded by the Ministry of Education, Science, Research and Sport of the Slovak Republic.

Data Availability Statement: Data are contained within the article.

Acknowledgments: As the authors of this article, we would like to thank the support of the project AMTRteam (Advanced Manufacturing Technology Research Team) awarded by the Ministry of Education, Science, Research and Sport of the Slovak Republic.

Conflicts of Interest: The authors declare no conflicts of interest.

References

1. Jurko, J.; Miškiv-Pavlik, M.; Hladký, V.; Lazorič, P.; Michalík, P.; Petruška, I. Measurement of the Machined Surface Diameter by a Laser Triangulation Sensor and Optimization of Turning Conditions Based on the Diameter Deviation and Tool Wear by GRA and ANOVA. *Appl. Sci.* **2022**, *12*, 5266. [[CrossRef](#)]
2. Powell, D.; Magnanini, M.C.; Colledani, M.; Myklebust, O. Advancing Zero Defect Manufacturing: A State-of-the-Art Perspective and Future Research Directions. *Comput. Ind.* **2022**, *136*, 103596. [[CrossRef](#)]
3. Bagaber, S.A.; Yusoff, A.R. Multi-objective optimization of cutting parameters to minimize power consumption in dry turning of stainless steel 316. *J. Clean. Prod.* **2017**, *157*, 30–46. [[CrossRef](#)]

4. Chen, C.; Leach, R.; Wang, J.; Liu, X.; Jiang, X.; Lu, W. Locally adaptive thresholding centroid localization in confocal microscopy. *Opt. Lett.* **2021**, *46*, 1616–1619. [[CrossRef](#)] [[PubMed](#)]
5. Wang, Z.; Wang, T.; Yang, Y.; Yang, Y.; Mi, X.; Wang, J. Precise Two-Dimensional Tilt Measurement Sensor with Double-Cylindrical Mirror Structure and Modified Mean-Shift Algorithm for a Confocal Microscopy System. *Sensors* **2022**, *22*, 6794. [[CrossRef](#)]
6. Saeidi Aminabadi, S.; Jafari-Tabrizi, A.; Gruber, D.P.; Berger-Weber, G.; Friesenbichler, W. An Automatic, Contactless, High-Precision, High-Speed Measurement System to Provide In-Line, As-Molded Three-Dimensional Measurements of a Curved-Shape Injection-Molded Part. *Technologies* **2022**, *10*, 95. [[CrossRef](#)]
7. Liu, Y.; Zhang, Q.; Liu, Y.; Yu, X.; Hou, Y.; Chen, W. High-Speed 3D Shape Measurement Using a Rotary Mechanical Projector. *Opt. Express* **2021**, *29*, 7885–7903. [[CrossRef](#)]
8. Yang, Y.; Dong, Z.; Meng, Y.; Shao, C. Data-Driven Intelligent 3D Surface Measurement in Smart Manufacturing: Review and Outlook. *Machines* **2021**, *9*, 13. [[CrossRef](#)]
9. Ruan, Y.; Xue, M.; Teng, J.; Wu, Y.; Shi, M. Horizontal Oxidation Diffusion Behavior of MEMS-Based Tungsten-Rhenium Thin Film Thermocouples. *Materials* **2022**, *15*, 5071. [[CrossRef](#)]
10. Andrea, L.M.; James, W.M.; Zhirong, L.; Alistair, S.; Jose, A.R.; Dragos, A.A.; Mark, C.H.; Adam, T.C. Surface integrity in metal machining-Part II: Functional performance. *Int. J. Mach. Tools Manuf.* **2021**, *164*, 103718. [[CrossRef](#)]
11. Liu, G.; Huang, C.; Zhao, B.; Wang, W.; Sun, S. Effect of Machined Surface Integrity on Fatigue Performance of Metal Workpiece: A Review. *Chin. J. Mech. Eng.* **2021**, *34*, 118. [[CrossRef](#)]
12. Felho, C.; Varga, G. Theoretical Roughness Modeling of Hard Turned Surfaces Considering Tool Wear. *Machines* **2022**, *10*, 188. [[CrossRef](#)]
13. Kovaci, H.; Bozkurt, Y.; Yetim, A.; Aslan, M.; Çelik, A. The effect of surface plastic deformation produced by shot peening on corrosion behavior of a low-alloy steel. *Surf. Coat. Technol.* **2019**, *360*, 78–86. [[CrossRef](#)]
14. Böhm, M.; Kowalski, M.; Niesłony, A. Influence of the Elastoplastic Strain on Fatigue Durability Determined with the Use of the Spectral Method. *Materials* **2020**, *13*, 423. [[CrossRef](#)]
15. Xiong, Y.; Yue, Y.; He, T.; Lu, Y.; Ren, F.; Cao, W. Effect of Rolling Temperature on Microstructure Evolution and Mechanical Properties of AISI316LN Austenitic Stainless Steel. *Materials* **2018**, *11*, 1557. [[CrossRef](#)] [[PubMed](#)]
16. Kiran, B.; Nagaraju, D. Simulation and experimental study on the effect of surface residual stresses in dry orthogonal micro turning sample. *Aust. J. Mech. Eng.* **2022**, *21*, 1396–1408. [[CrossRef](#)]
17. Yu, C.; Shiue, R.-K.; Chen, C.; Tsay, L.-W. Effect of Low-Temperature Sensitization on Hydrogen Embrittlement of 301 Stainless Steel. *Metals* **2017**, *7*, 58. [[CrossRef](#)]
18. Wisley, F.S.; Julius, S.; Leonardo, R.R.D.S.; Álisson, R.M.; Jawahir, I.S. A review of surface integrity in machining of hardened steels. *J. Manuf. Process* **2020**, *58*, 136–162. [[CrossRef](#)]
19. Moravčíková, J.; Moravčík, R.; Palcut, M. Effect of Heat Treatment on the Resulting Dimensional Characteristics of the C45 Carbon Steel after Turning. *Metals* **2022**, *12*, 1899. [[CrossRef](#)]
20. Chung, Y.-H.; Chen, T.-C.; Lee, H.-B.; Tsay, L.-W. Effect of Micro-Shot Peening on the Fatigue Performance of AISI 304 Stainless Steel. *Metals* **2021**, *11*, 1408. [[CrossRef](#)]
21. Groeb, M.; Hagelüken, L.; Groeb, J.; Ensinger, W. Experimental Analysis of Ductile Cutting Regime in Face Milling of Sintered Silicon Carbide. *Materials* **2022**, *15*, 2409. [[CrossRef](#)]
22. Peng, C.-H.; Hou, P.-Y.; Lin, W.-S.; Shen, P.-K.; Huang, H.-H.; Yeh, J.-W.; Yen, H.-W.; Huang, C.-Y.; Tsai, C.-W. Investigation of Microstructure and Wear Properties of Precipitates-Strengthened Cu-Ni-Si-Fe Alloy. *Materials* **2023**, *16*, 1193. [[CrossRef](#)]
23. Zhu, P.; Zhao, Y.; Agarwal, S.; Henry, J.; Zinkle, S.J. Toward accurate evaluation of bulk hardness from nanoindentation testing at low indent depths. *Mater. Des.* **2022**, *213*, 110317. [[CrossRef](#)]
24. Clayton, J.D.; Casem, D.T.; Lloyd, J.T.; Retzlaff, E.H. Toward Material Property Extraction from Dynamic Spherical Indentation Experiments on Hardening Polycrystalline Metals. *Metals* **2023**, *13*, 276. [[CrossRef](#)]
25. Luo, Q.; Kitchen, M. Microhardness, Indentation Size Effect and Real Hardness of Plastically Deformed Austenitic Hadfield Steel. *Materials* **2023**, *16*, 1117. [[CrossRef](#)]
26. Nix, W.D.; Gao, H. Indentation size effects in crystalline materials: A law for strain gradient plasticity. *J. Mech. Phys. Solids* **1998**, *46*, 411–425. [[CrossRef](#)]
27. Sarangi, S.S.; Lavakumar, A.; Singh, P.K.; Katiyar, P.K.; Ray, R.K. Indentation size effect in steels with different carbon contents and microstructures. *Mater. Sci. Technol.* **2023**, *39*, 338–346. [[CrossRef](#)]
28. Song, P.; Yabuuchi, K.; Spaetig, P. Insights into hardening, plastically deformed zone and geometrically necessary dislocations of two ion-irradiated FeCrAl (Zr)-ODS ferritic steels: A combined experimental and simulation study. *Acta Mater.* **2022**, *234*, 117991. [[CrossRef](#)]
29. Broitman, E. Indentation Hardness Measurements at Macro-, Micro-, and Nanoscale: A Critical Overview. *Tribol. Lett.* **2017**, *65*, 23. [[CrossRef](#)]
30. Balos, S.; Rajnovic, D.; Sidjanin, L.; Cekic, O.E.; Moraca, S.; Trivkovic, M.; Dedic, M. Vickers hardness indentation size effect in selective laser melted MSI maraging steel. *J. Mech. Eng. Sci.* **2021**, *235*, 1724–1730. [[CrossRef](#)]
31. Das, A.; Altstadt, E.; Kaden, C.; Kapoor, G.; Akhmadaliev, S.; Bergner, F. Nanoindentation Response of Ion-Irradiated Fe, Fe-Cr Alloys and Ferritic-Martensitic Steel Eurofer 97: The Effect of Ion Energy. *Front. Mater.* **2022**, *8*, 811851. [[CrossRef](#)]

32. Amanov, A.; Karimbaev, R.; Maleki, E.; Okan, U.; Young-Sik, P.; Amanov, T. Effect of combined shot peening and ultrasonic nanocrystal surface modification processes on the fatigue performance of AISI 304. *Surf. Coat. Technol.* **2019**, *358*, 695–705. [[CrossRef](#)]
33. Baleani, A.; Paone, N.; Gladines, J.; Vanlanduit, S. Design and Metrological Analysis of a Backlit Vision System for Surface Roughness Measurements of Turned Parts. *Sensors* **2023**, *23*, 1584. [[CrossRef](#)]
34. Jayabarathi, S.B.; Ratnam, M.M. Comparison of Correlation between 3D Surface Roughness and Laser Speckle Pattern for Experimental Setup Using He-Ne as Laser Source and Laser Pointer as Laser Source. *Sensors* **2022**, *22*, 6003. [[CrossRef](#)] [[PubMed](#)]
35. dos Santos Motta Neto, W.; Leal, J.E.S.; Arantes, L.J.; Arencibia, R.V. The Effect of Stylus Tip Radius on Ra, Rq, Rp, Rv, and Rt Parameters in Turned and Milled Samples. *Int. J. Adv. Manuf. Technol.* **2018**, *99*, 1979–1992. [[CrossRef](#)]
36. Maruda, R.W.; Krolczyk, G.M.; Wojciechowski, S.; Powalka, B.; Klos, S.; Szczotkarz, N.; Matuszak, M.; Khanna, N. Evaluation of turning with different cooling-lubricating techniques in terms of surface integrity and tribologic properties. *Tribol. Int.* **2020**, *148*, 106334. [[CrossRef](#)]
37. Yıldırım, Ç.V.; Kivak, T.; Sarıkaya, M.; Şirin, Ş. Evaluation of tool wear, surface roughness/topography and chip morphology when machining of Ni-based alloy 625 under MQL, cryogenic cooling and CryoMQL. *J. Mater. Res. Technol.* **2020**, *9*, 2079–2092. [[CrossRef](#)]
38. Leksycki, K.; Feldshtein, E.; Lisowicz, J.; Chudy, R.; Mrugalski, R. Cutting Forces and Chip Shaping When Finish Turning of 17-4 PH Stainless Steel under Dry, Wet, and MQL Machining Conditions. *Metals* **2020**, *10*, 1187. [[CrossRef](#)]
39. Yadav, S.P.; Pawade, R.S. Manufacturing Methods Induced Property Variations in Ti6Al4V Using High-Speed Machining and Additive Manufacturing (AM). *Metals* **2023**, *13*, 287. [[CrossRef](#)]
40. Naeim, N.; AbouEleaz, M.A.; Elkaseer, A. Experimental Investigation of Surface Roughness and Material Removal Rate in Wire EDM of Stainless Steel 304. *Materials* **2023**, *16*, 1022. [[CrossRef](#)]
41. Abu Qudeiri, J.E.; Saleh, A.; Ziout, A.; Mourad, A.-H.I.; Abidi, M.H.; Elkaseer, A. Advanced Electric Discharge Machining of Stainless Steels: Assessment of the State of the Art, Gaps and Future Prospect. *Materials* **2019**, *12*, 907. [[CrossRef](#)] [[PubMed](#)]
42. Nguyen, D.-K.; Huang, H.-C.; Feng, T.-C. Prediction of Thermal Deformation and Real-Time Error Compensation of a CNC Milling Machine in Cutting Processes. *Machines* **2023**, *11*, 248. [[CrossRef](#)]
43. Chodór, J.; Kukielka, L.; Chomka, G.; Bohdal, L.; Patyk, R.; Kowalik, M.; Trzepieciński, T.; Radchenko, A.M. Using the FEM Method in the Prediction of Stress and Deformation in the Processing Zone of an Elastic/Visco-Plastic Material during Diamond Sliding Burnishing. *Appl. Sci.* **2023**, *13*, 1963. [[CrossRef](#)]
44. Tagiuri, Z.A.M.; Dao, T.-M.; Samuel, A.M.; Songmene, V. Numerical Prediction of the Performance of Chamfered and Sharp Cutting Tools during Orthogonal Cutting of AISI 1045 Steel. *Processes* **2022**, *10*, 2171. [[CrossRef](#)]
45. Wang, R.; Yang, D.; Wang, W.; Wei, F.; Lu, Y.; Li, Y. Tool Wear in Nickel-Based Superalloy Machining: An Overview. *Processes* **2022**, *10*, 2380. [[CrossRef](#)]
46. Hailong, M.; Aijun, T.; Shubo, X.; Tong, L. Finite Element Simulation of Bending Thin-Walled Parts and Optimization of Cutting Parameters. *Metals* **2023**, *13*, 115. [[CrossRef](#)]
47. Dyl, T. The Designation Degree of Tool Wear after Machining of the Surface Layer of Duplex Stainless Steel. *Materials* **2021**, *14*, 6425. [[CrossRef](#)]
48. Wang, W.; Wang, B.; Liu, B.; Gao, H.; Wei, Z. Machinability and chip morphology evolution of hardened stainless steel using liquid nitrogen cryogenic. *Int. J. Adv. Manuf. Technol.* **2022**, *125*, 967–987. [[CrossRef](#)]
49. Królczyk, G.M.; Niesłony, P.; Legutko, S. Determination of tool life and research wear during duplex stainless steel turning. *Arch. Civ. Mech. Eng.* **2015**, *15*, 347–354. [[CrossRef](#)]
50. Królczyk, G.M.; Niesłony, P.; Legutko, S.; Hloch, S.; Samardzic, I. Investigation of selected surface integrity features of duplex stainless steel after turning. *Metalurgija* **2015**, *54*, 91–94.
51. Sarıkaya, M.; Gupta, M.K.; Tomaz, I.; Pimenov, D.Y.; Kuntoğlu, M.; Khanna, N.; Yıldırım, Ç.V.; Krolczyk, G.M. A state-of-the-art review on tool wear and surface integrity characteristics in machining of superalloys. *CIRP J. Manuf. Sci. Technol.* **2021**, *35*, 624–658. [[CrossRef](#)]
52. Dzierwa, A.; Markopoulos, A.P. Influence of Ball-Burnishing Process on Surface Topography Parameters and Tribological Properties of Hardened Steel. *Machines* **2019**, *7*, 11. [[CrossRef](#)]
53. Khanna, N.; Airao, J.; Gupta, M.K.; Song, Q.; Liu, Z.; Mia, M.; Maruda, R.; Krolczyk, G. Optimization of Power Consumption Associated with Surface Roughness in Ultrasonic Assisted Turning of Nimonic-90 Using Hybrid Particle Swarm-Simplex Method. *Materials* **2019**, *12*, 3418. [[CrossRef](#)]
54. Sousa, V.F.C.; Silva, F.J.G.; Lopes, H.; Casais, R.C.B.; Baptista, A.; Pinto, G.; Alexandre, R. Wear Behavior and Machining Performance of TiAlSiN-Coated Tools Obtained by dc MS and HiPIMS: A Comparative Study. *Materials* **2021**, *14*, 5122. [[CrossRef](#)] [[PubMed](#)]
55. Wojciechowski, S.; Królczyk, G.M.; Maruda, R.W. Advances in Hard-to-Cut Materials: Manufacturing, Properties, Process Mechanics and Evaluation of Surface Integrity. *Materials* **2020**, *13*, 612. [[CrossRef](#)]
56. Cardoso, L.G.; Madeira, D.S.; Ricomini, T.E.P.A.; Miranda, R.A.; Brito, T.G.; Paiva, E.J. Optimization of machining parameters using response surface methodology with desirability function in turning duplex stainless steel UNS S32760. *Int. J. Adv. Manuf. Technol.* **2021**, *117*, 1633–1644. [[CrossRef](#)]

57. Cao, Z.-M.; Wu, Y.; Han, J. Roundness deviation evaluation method based on statistical analysis of local least square circles, *Meas. Sci. Technol.* **2017**, *28*, 10. [[CrossRef](#)]
58. Kumar, S.; Riyaz, A.M.; Marulaiah, L.; Manjunatha, L. Investigation of machinability characteristics on C45 steel alloy while turning with untreated and cryotreated M2 HSS cutting tools. *ARN J. Eng. Appl. Sci.* **2019**, *14*, 307–317. [[CrossRef](#)]
59. Sivaprakash, E.; Aswin, S.; Dhanaruban, D.; Dinesh, G.; Inbamathi, M. Machining Character Analysis of Coated and Uncoated End Mill on Heat Treated C45 Steel. *Int. J. Res. Appl. Sci. Eng. Technol.* **2022**, *10*, 2708–2713. [[CrossRef](#)]
60. Usca, Ü.A. The Effect of Cellulose Nanocrystal-Based Nanofluid on Milling Performance: An Investigation of Dillimax 690T. *Polymers* **2023**, *15*, 4521. [[CrossRef](#)]
61. Tuan, B.; Hai, N.; Kien, L.; Hai, N. Investigation of surface topography in ultrasonic-assisted turning of C45 carbon steel. *Jpn. J. Appl. Phys.* **2023**, *63*, 016501. [[CrossRef](#)]
62. SreeramaReddy, T.V.; Sornakumar, T.; Venkatarama Reddy, M.; Venkatram, R. Machinability of C45 steel with deep cryogenic treated tungsten carbide cutting tool inserts. *Int. J. Refract. Met. Hard Mater.* **2009**, *27*, 181–185. [[CrossRef](#)]
63. Huang, G.; Bai, J.; Feng, F.; Zeng, L.; Feng, P.; Li, X. A Hybrid Strategy for Profile Measurement of Micro Gear Teeth. *Micromachines* **2023**, *14*, 1729. [[CrossRef](#)]
64. Lishchenko, N.; O'Donnell, G.E.; Culleton, M. Contactless Method for Measurement of Surface Roughness Based on a Chromatic Confocal Sensor. *Machines* **2023**, *11*, 836. [[CrossRef](#)]
65. Cheng, F.; Fu, S.; Chen, Z. Surface Texture Measurement on Complex Geometry Using Dual-Scan Positioning Strategy. *Appl. Sci.* **2020**, *10*, 8418. [[CrossRef](#)]
66. ISO 3685:1993 (E); Tool-Life Testing with Single-Point Turning Tools. International Organization for Standardization: Geneva, Switzerland, 1993.
67. Belavendram, N. *Quality by Design: Taguchi Techniques for Industrial Experimentation*; Prentice Hall: London, UK, 1995; ISBN 9780131863620.
68. Antony, J.; Kaye, M. The Taguchi Approach to Industrial Experimentation. In *Experimental Quality*; Springer: Boston, MA, USA, 2000. [[CrossRef](#)]
69. Taguchi, G. *System of Experimental Design: Engineering Methods to Optimize Quality and Minimize Costs*; UNIPUB/Kraus International Publications: White Plains, NY, USA, 1987; p. 1189. ISBN 9780941243001.
70. Sap, E.; Usca, Ü.A.; Gupta, M.K.; Kuntoğlu, M.; Sarıkaya, M.; Pimenov, D.Y.; Mia, M. Parametric Optimization for Improving the Machining Process of Cu/Mo-SiCP Composites Produced by Powder Metallurgy. *Materials* **2021**, *14*, 1921. [[CrossRef](#)] [[PubMed](#)]
71. Vora, J.; Chaudhari, R.; Patel, C.; Pimenov, D.Y.; Patel, V.K.; Giasin, K.; Sharma, S. Experimental Investigations and Pareto Optimization of Fiber Laser Cutting Process of Ti6Al4V. *Metals* **2021**, *11*, 1461. [[CrossRef](#)]
72. Selvam, M.D.; Senthil, P. Investigation on the effect of turning operation on surface roughness of hardened C45 carbon steel. *Aust. J. Mech. Eng.* **2016**, *14*, 131–137. [[CrossRef](#)]
73. Singh, M.; Garg, H.K.; Maharana, S.; Yadav, A.; Singh, R.; Maharana, P.; Nguyen, T.V.T.; Yadav, S.; Loganathan, M.K. An Experimental Investigation on the Material Removal Rate and Surface Roughness of a Hybrid Aluminum Metal Matrix Composite (Al6061/SiC/Gr). *Metals* **2021**, *11*, 1449. [[CrossRef](#)]
74. Prakash, K.S.; Gopal, P.; Karthik, S. Multi-objective optimization using Taguchi based grey relational analysis in turning of Rock dust reinforced Aluminum MMC. *Measurement* **2020**, *157*, 107664. [[CrossRef](#)]
75. Akhtar, M.N.; Sathish, T.; Mohanavel, V.; Afzal, A.; Arul, K.; Ravichandran, M.; Rahim, I.A.; Alhady, S.S.N.; Bakar, E.A.; Saleh, B. Optimization of Process Parameters in CNC Turning of Aluminum 7075 Alloy Using L27 Array-Based Taguchi Method. *Materials* **2021**, *14*, 4470. [[CrossRef](#)] [[PubMed](#)]
76. Krolczyk, J.B.; Maruda, R.W.; Krolczyk, G.M.; Wojciechowski, S.; Gupta, M.K.; Korkmaz, M.E. Investigations on surface induced tribological characteristics in MQCL assisted machining of duplex stainless steel. *J. Mater. Res. Technol.* **2022**, *18*, 2754–2769. [[CrossRef](#)]
77. Fratila, D.; Caizar, C. Application of Taguchi method to selection of optimal lubrication and cutting conditions in face milling of AlMg3. *J. Clean. Prod.* **2011**, *19*, 640–645. [[CrossRef](#)]
78. Lubis, S.M.; Darmawan'Adianto, S. Effect of cutting speed on temperature cutting tools and surface roughness of AISI 4340 steel. *IOP Conf. Ser. Mater. Sci. Eng.* **2019**, *508*, 012053. [[CrossRef](#)]
79. Gunjal, S.U.; Patil, N.G. Experimental Investigations into Turning of Hardened AISI 4340 Steel using Vegetable based Cutting Fluids under Minimum Quantity Lubrication. *Procedia Manuf.* **2018**, *20*, 18–23. [[CrossRef](#)]
80. Fnides, M. Optimization and Mathematical Modelling of Surface Roughness Criteria and Material Removal Rate when Milling C45 Steel using RSM and Desirability Approach. *J. Mech. Eng.* **2023**, *20*, 173–197. [[CrossRef](#)]
81. Jamil, M.; Khan, A.M.; He, N.; Li, L.; Zhao, W.; Sarfraz, S. Multi-response optimisation of machining aluminium-6061 under eco-friendly electrostatic minimum quantity lubrication environment. *Int. J. Mach. Mach. Mater.* **2019**, *21*, 459–479. [[CrossRef](#)]
82. Mia, M.; Gupta, M.K.; Lozano, J.A.; Carou, D.; Pimenov, D.Y.; Królczyk, G.; Khan, A.M.; Dhar, N.R. Multi-objective optimization and life cycle assessment of eco-friendly cryogenic N2 assisted turning of Ti-6Al-4V. *J. Clean. Prod.* **2019**, *210*, 121–133. [[CrossRef](#)]
83. Pu, Y.; Zhao, Y.; Meng, J.; Zhao, G.; Zhang, H.; Liu, Q. Process Parameters Optimization Using Taguchi-Based Grey Relational Analysis in Laser-Assisted Machining of Si₃N₄. *Materials* **2021**, *14*, 529. [[CrossRef](#)]
84. Mufarrih, A.; Istiqlaliyah, H.; Ilha, M. Optimization of Roundness, MRR and Surface Roughness on Turning Process using Taguchi-GRA. *J. Phys. Conf. Ser.* **2019**, *1179*, 012099. [[CrossRef](#)]

85. Jin, L.; Wang, G.; Deng, J.; Li, Z.; Zhu, M.; Wang, R. A New Model for Cleaning Small Cuttings in Extended-Reach Drilling Based on Dimensional Analysis. *Appl. Sci.* **2023**, *13*, 12118. [[CrossRef](#)]
86. Tian, P.; He, L.; Zhou, T.; Du, F.; Zou, Z.; Zhou, X. Experimental characterization of the performance of MQL-assisted turning of solution heat-treated and aged Inconel 718 alloy. *Int. J. Adv. Manuf. Technol.* **2023**, *125*, 3839–3851. [[CrossRef](#)]
87. Thakur, A.; Gangopadhyay, S. State-of-the-art in surface integrity in machining of nickel-based super alloys. *Int. J. Mach. Tool. Manuf.* **2016**, *100*, 25–54. [[CrossRef](#)]
88. Kivak, T. Optimization of surface roughness and flank wear using the Taguchi method in milling of Hadfield steel with PVD and CVD coated inserts. *Measurement* **2014**, *50*, 19–28. [[CrossRef](#)]
89. Debnath, S.; Reddy, M.M.; Yi, Q.S. Influence of cutting fluid conditions and cutting parameters on surface roughness and tool wear in turning process using Taguchi method. *Measurement* **2016**, *78*, 111–119. [[CrossRef](#)]
90. Maruda, R.W.; Krolczyk, G.M.; Feldshtein, E.; Nieslony, P.; Tyliszczak, B.; Pusavec, F. Tool wear characterizations in finish turning of AISI 1045 carbon steel for MQCL conditions. *Wear* **2017**, *372–373*, 54–67. [[CrossRef](#)]
91. Klocke, F. *Fertigungsverfahren 1*; Springer Science and Business Media LLC: Dordrecht, The Netherlands, 2018; ISBN 978-3-662-54206-4. [[CrossRef](#)]
92. Hou, Z.; Yuan, Y.; Chen, Y.; Jiang, E.; Wang, H.; Zhang, X. A Review of the Settling Law of Drill Cuttings in Drilling Fluids. *Processes* **2023**, *11*, 3165. [[CrossRef](#)]
93. Yin, W.-H.; Yue, H.; Wang, X. A Study on the Depositional Law of Road Cutting in the Tengger Desert. *Appl. Sci.* **2023**, *13*, 11967. [[CrossRef](#)]
94. Jurko, J.; Miškov-Pavlik, M.; Husár, J.; Michalik, P. Turned Surface Monitoring Using a Confocal Sensor and the Tool Wear Process Optimization. *Processes* **2022**, *10*, 2599. [[CrossRef](#)]

Disclaimer/Publisher’s Note: The statements, opinions and data contained in all publications are solely those of the individual author(s) and contributor(s) and not of MDPI and/or the editor(s). MDPI and/or the editor(s) disclaim responsibility for any injury to people or property resulting from any ideas, methods, instructions or products referred to in the content.